BIOCHEMISTRY
including biophysical chemistry & molecular biology

Article

pubs.acs.org/biochemistry

Amino Acid Oxidation of *Candida antarctica* Lipase B Studied by Molecular Dynamics Simulations and Site-Directed Mutagenesis

Mehdi Irani,[†,∥] Ulrika Törnvall,[‡,⊥] Samuel Genheden,[†] Marianne Wittrup Larsen,[§] Rajni Hatti-Kaul,[‡] and Ulf Ryde*[,†]

[†]Department of Theoretical Chemistry, Lund University, Chemical Centre, P.O. Box 124, SE-221 00 Lund, Sweden

[‡]Department of Biotechnology, Lund University, Chemical Centre, P.O. Box 124, SE-221 00 Lund, Sweden

[§]Department of Biochemistry, School of Biotechnology, Royal Institute of Technology, AlbaNova University Center, 106 91 Stockholm, Sweden

Supporting Information

ABSTRACT: Molecular dynamics simulations have been performed on lipase B from *Candida antarctica* (CalB) in its native form and with one or two oxidized residues, either methionine oxidized to methionine sulfoxide, tryptophan oxidized to 5-hydroxytryptophan, or cystine oxidized to a pair of cysteic acid residues. We have analyzed how these oxidations affect the general structure of the protein as well as the local structure around the oxidized amino acid and the active site. The results indicate that the methionine and tryptophan oxidations led to rather restricted changes in the structure, whereas the oxidation of cystines, which also caused cleavage of the cystine S−S linkage, gave rise to larger changes in the protein structure. Only two oxidized residues caused significant changes in the structure of the active site, viz., those of the Cys-22/64 and Cys-216/258 pairs. Site-directed mutagenesis studies were also performed. Two variants showed a behavior similar to that of native CalB (M83I and M129L), whereas W155Q and M72S had severely decreased specific activity. M83I had a slightly higher thermostability than native CalB. No significant increase in stability toward hydrogen peroxide was observed. The same mutants were also studied by molecular dynamics. Even though no significant increase in stability toward hydrogen peroxide was observed, the results from simulations and site-directed mutagenesis give some clues about the direction of further work on stabilization.

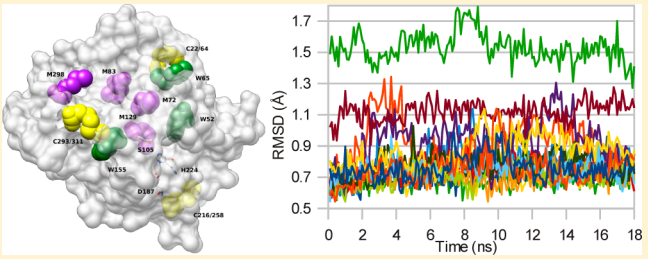

Industrial biotechnology is an important tool in the chemical industry for facilitating a paradigm shift from fossil-based to bio-based production and for providing selective and energy-efficient process alternatives to chemical synthesis. Despite many advantages of biocatalysis, one major limitation to its widespread application has been access to suitable biocatalysts with respect to activity and stability under process conditions. Oxidation has been identified as one of the major degradation pathways in proteins and peptides, resulting in a loss of activity.[1]

Epoxidation is among the most important reactions in organic chemistry. Epoxides are important building blocks in organic synthesis and provide a variety of industrially important products, e.g., polyurethane, cross-linkers for powder coatings, PVC plasticizers, and surfactants.[2−4] Different enzymes, including lipases, chloroperoxidases, cytochrome P450 monooxygenases, and epoxide hydrolases, have been used to catalyze epoxidation reactions, among which lipases have shown several promising features.[5−7] The reactions catalyzed by peroxidases and lipases use hydrogen peroxide as the oxygen donor. Many lipases accept hydrogen peroxide as a nucleophile and catalyze the formation of peroxycarboxylic acids, from which one of the oxygen atoms is spontaneously transferred to the double bond of a substrate to form an epoxide,[8] as shown in Figure 1.

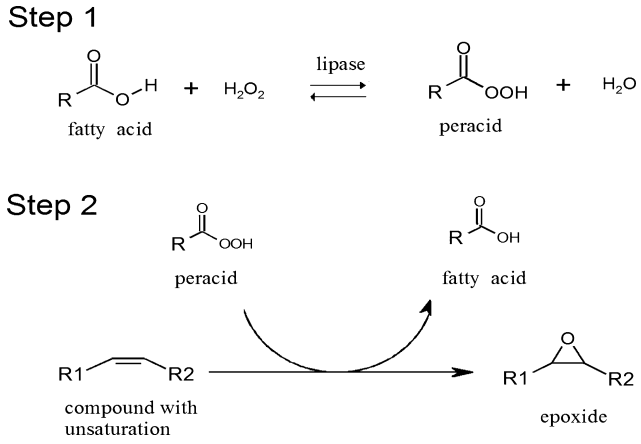

Figure 1. Schematic view of the epoxidation reaction catalyzed by lipases.

Lipase B from the basidiomycetous yeast *Candida* (also called *Pseudozyma*) *antarctica* (CalB)[9] is one of the most widely used

Received: September 24, 2012
Revised: December 21, 2012
Published: January 18, 2013

biocatalysts in industry.[10] The enzyme has a molecular mass of 33 kDa and a pI of 6.0. The structure of CalB has been resolved by X-ray diffraction.[11,12] The polypeptide chain consists of 317 amino acids, which fold into a α/β-hydrolase fold. Like other lipases, CalB is a serine hydrolase, and the active site contains a Ser−His−Asp catalytic triad. However, unlike other lipases, CalB does not seem to possess a lid domain.[13] Furthermore, it has a limited amount of space available in the active-site pocket and thus exhibits a high degree of selectivity. CalB has three disulfide bridges and is glycosylated at Asn-74.[12] The enzyme has been expressed in *Aspergillus oryzae*, *Pichia pastoris*, and *Escherichia coli*.[14]

For use in organic synthesis, the enzyme may be immobilized onto a solid matrix. An earlier study has shown immobilized CalB to be the most efficient lipase for the synthesis of peroxy acid.[6] This might be because of a higher resistance of CalB to oxidation by hydrogen peroxide compared to those of the other lipases, which in turn could be related to a smaller number of oxidation-sensitive amino acids in the enzyme. However, it has been shown that Novozym435 (CalB adsorbed to an acrylic copolymer) becomes inactive during its use as a catalyst in epoxidation processes under solvent-free conditions[6] and that the rate of enzyme inactivation is related to the concentration of H_2O_2 and temperature.[15]

CalB has one His residue, four Met residues, five Trp residues, and eight Tyr residues, i.e., residues that could be expected to be sensitive to oxidation. To improve the stability of CalB, it is important to gain an understanding of the effect of oxidation on the enzyme structure and dynamics. Recently, the oxidation of CalB with hydrogen peroxide has been investigated by mass spectrometry.[16,17] The results showed that Met-298 was the most prone to oxidation. However, oxidation of the other three Met residues (Met-72, -83, and -129), two Trp residues (Trp-65 and -155), and all three disulfide bridges (Cys-22, -64, -216, -258, -293, and -311) was also detected (the locations of the various oxidized residues are indicated in Figure 2). On the other hand, the active-site His residue was not oxidized. Extended exposure to H_2O_2 led to partial fragmentation of the backbone and extensive changes in the structure of the protein.

A logical remedy to the oxidation damage of CalB is to replace amino acids that are easily oxidized by more resistant amino acids using mutagenesis. However, this is necessary only if the oxidations affect the structure or activity of the enzyme. Therefore, in this work, we perform molecular dynamics (MD) simulations of CalB with various oxidized amino acids. The aim is to examine how the various oxidations affect the general structure of the protein, as well as the local structure of the active site. To further investigate the effect of oxidation and to verify the MD simulations, site-directed mutagenesis of CalB is also performed, and the corresponding mutants are expressed and tested for activity and stability. In addition, these mutants are also studied by MD simulations.

METHODS

Molecular Dynamics Simulations. The MD simulations were based on a 1.55 Å crystal structure of CalB (Protein Data Bank entry 1TCA).[11] The protein was solvated in a truncated octahedral box extending at least 9 Å on all sides of the protein, giving a total of 7988 water molecules and ∼28600 atoms. All Lys and Arg residues were assumed to be positively charged, and all Asp and Glu residues were negatively charged. The only exception was Asp-134, which is deeply buried in the protein, close to the active site. It was modeled as protonated and neutral in all simulations, except one (WtD). This assignment was confirmed by PROPKA.[18] All six Cys residues were involved in disulfide linkages. The only His residue in CalB is His-224, which together with Ser-105 and Asp-187 is part of the catalytic triad. We studied the free enzyme without any bound substrate. Therefore, we assumed that Asp-187 was deprotonated, accepting a hydrogen bond from ND1 of His-224, whereas the NE2 atom was deprotonated and accepted a hydrogen bond from Ser-105 at the start of the simulations.

Sixteen different simulations were performed in this study. Two involved the native (wild-type) protein, and they differed in the protonation state of Asp-134, protonated (WtP) or deprotonated (WtD). In 10 simulations, Asp-134 was protonated and one or two amino acids were oxidized, viz., Met-72, -83,

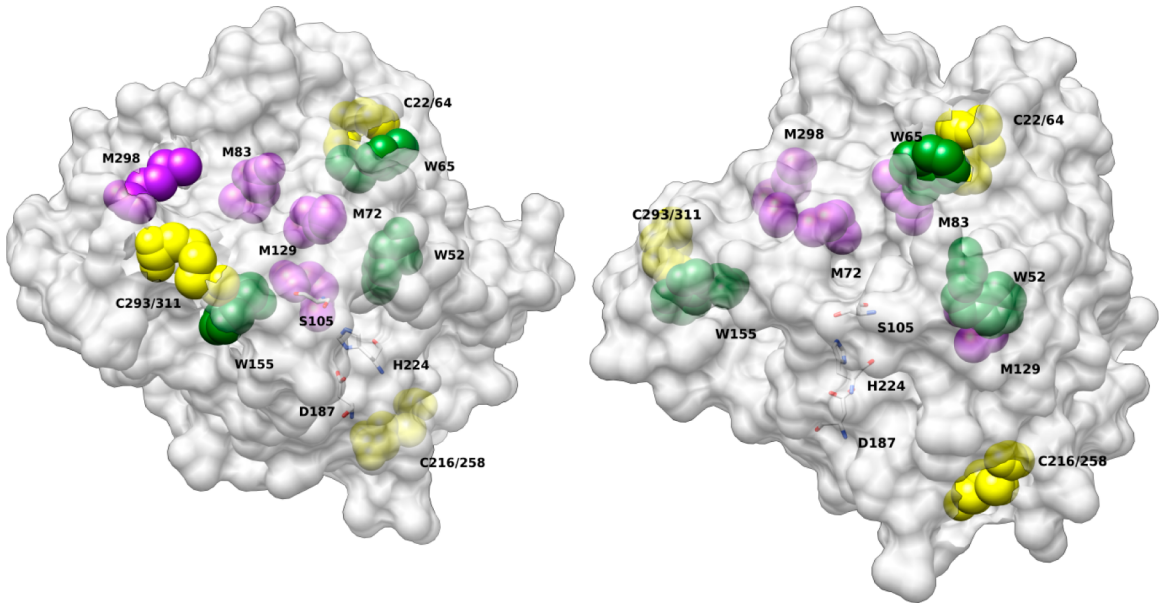

Figure 2. CalB from two different angles with the oxidized residues as well as the catalytic triad marked. A semitransparent surface of the protein is shown, highlighting the solvent accessibility of the oxidized residues.

dx.doi.org/10.1021/bi301298m | *Biochemistry* 2013, 52, 1280−1289

-129, and -298, Trp-52, -65, and -155, or the two Cys residues of the former disulfide bridges, Cys-22 and -64, Cys-216 and -258, or Cys-293 and -311. These simulations are denoted M72, M83, M129, M298, W52, W65, W155, C22/64, C216/258, and C293/311, respectively. The location and solvent accessibility of the various oxidized residues are indicated in Figure 2. In addition, four mutants were constructed, M72S, M83I, M129L, and W155Q, by cutting away the modified atoms and adding the new ones by the tleap module in Amber 10.[19] In all mutants, Asp-134 was protonated.

The simulations were started by a 240 ps simulated annealing MD in which only the added water molecules and hydrogen atoms were allowed to move, while the temperature was first kept at 370 K and then slowly reduced to 0 K. It was followed by 10000 steps of minimization. Then, all atoms were allowed to move; the temperature was set to 300 K, and a 500 ps equilibration was run with a constant pressure (1 atm). Finally, a 18 ns production simulation was run under the same conditions. The C216/258 and C293/311 simulations showed extensive variation in some of the properties during these 18 ns simulations. Therefore, these simulations were extended to 33 ns, and the analysis is based on the last 18 ns of the simulations.

All MD simulations were run using the sander module of Amber 10.[19] The temperature was kept constant at 300 K using Langevin dynamics[20] with a collision frequency of 2.0 ps^{-1}, and the pressure was kept constant at 1 atm using a weak-coupling isotropic algorithm with a relaxation time of 1 ps.[21] Particle mesh Ewald summation with a fourth-order B spline interpolation and a tolerance of 10^{-5} was used to handle the long-range electrostatics.[22] The cutoff for nonbonded interactions was set to 8 Å, and the nonbonded pair list was updated every 50 fs. The SHAKE algorithm[23] was used to constrain bonds involving hydrogen atoms so that a 2 fs time step could be used.

The normal amino acids were described by the Amber 99SB force field[24] and water molecules with the TIP3P model.[25] Met was assumed to be oxidized to methionine sulfoxide, Cys to cysteic acid, and Trp to 5-hydroxytryptophan.[26] Charges for these residues were obtained by optimizing the isolated side chains at the Hartree−Fock/6-31G* level of theory. Then, the electrostatic potential was calculated with the same method in points sampled according to the Merz−Kollman scheme[27] using Gaussian 03.[28] Charges were fitted to these potentials using the RESP (restrained electrostatic potential) procedure using the antechamber program,[29] which also assigned AMBER atom types to the residues. Missing force field parameters were estimated from the harmonic frequencies calculated at the same level of theory using the Hess2FF approach.[30,31] AMBER topology and parameter files for these residues are included in the Supporting Information.

Six different properties were studied in the various simulations, viz., the radius of gyration, the root-mean-square deviation (rmsd) from the starting crystal structure, average *B* factors of the various residues, the S−S distances of the cystine disulfide pairs, and the hydrogen bond structure of the active site and around the oxidized amino acid. The properties were obtained with the AMBER ptraj module, analyzing trajectories with coordinates saved every 5 ps. The reported values are averages over these 3600 sets of coordinates, and uncertainties are the standard deviations over these sets divided by $(3600)^{1/2}$.

Construction of CalB M72S. CalB M83I, M129L, and W155Q were kind gifts from Novozymes A/S (Bagsvaerd, Denmark). CalB M72S was constructed using site-directed mutagenesis with plasmid pET-b(+) as a template.[32] Mutagenesis was performed using 45 ng of template plasmid, 10 pmol of oligonucleotides, 10 nmol of dNTP, 1 unit of *Phusion* DNA polymerase (Thermo Fisher Scientific, Waltham, MA), and 10 μL of 5× *Phusion* HF buffer in a final volume of 50 μL. After initial denaturation at 98 °C for 30 s, amplification was conducted by 30 cycles at 98 °C for 10 s followed by 72 °C for 3 min and 30 s. Hereafter, DpnI digestion of the template DNA was performed before 1 μL of the mixture was inserted by electroporation into *E. coli* Rosetta (DE3) cells and positive transformants were selected on LB plates containing ampicillin (100 μg/mL) and chloramphenicol (30 μg/mL). The point mutation was verified by DNA sequencing.

Protein Expression and Purification. For expression of CalB M72S in the periplasmic space variant in *E. coli*, 1 mL of overnight culture (10 mL in $LB_{Cam,Amp}$) was inoculated into 100 mL of $Superbroth_{Cam,Amp}$ medium. The culture was allowed to reach an OD_{600} of 0.5 before being induced with 1 mM isopropyl β-D-1-thiogalactopyranoside for 24 h at 16 °C. The protein was isolated by osmotic chock after the cells had been harvested by centrifugation (3300*g* and 4 °C for 15 min), via addition of 10 mL of buffer [30 mM Tris-HCl and 20% sucrose (pH 8)] and 20 μL of 0.5 M EDTA (final concentration of 1 mM) at pH 8 for 10 min. The supernatant was discarded after a second centrifugation step similar to the first, and the cells were resuspended in 10 mL of ice-cold 5 mM $MgSO_4$ and again incubated for 10 min. Finally, the periplasmic fraction was isolated by centrifugation of the cells at 21000*g* and 4 °C for 15 min. The protein was purified on His SpinTrap columns (GE Healthcare) according to the manufacturer's recommendations, followed by a desalting step on PD SpinTrap G-25 columns (GE Healthcare) also according to the manufacturer's recommendations.

Hydrogen Peroxide Treatment. Native CalB (filtered Lipozyme CALB L) and CalB M72S, M83I, M129L, and W155Q were diluted to equal concentrations, as determined by absorbance measurements at 280 nm, verified also by Bradford[33] and active-site titration.[16] The enzymes were treated with 0.2 and 2 M H_2O_2 at room temperature and 40 °C in a HTMR-131 thermomixer (HLC; 700 rpm). Enzyme samples (10 μL) were withdrawn after H_2O_2 treatment for 0−24 h and were mixed at a 1:1 ratio with cyclohexane.

Assay of Lipase Activity. Soluble lipase activity was examined by the esterification of decanoic acid (100 mM) with dodecanol (51 mM), dissolved in cyclohexane. Tetradecane was added to the substrate as an internal standard. Samples were withdrawn at appropriate time intervals and diluted with cyclohexane, and the composition was determined using a Varian 430 gas chromatograph (Varian Instrument group, Walnut Creek, CA). The analytes were separated on a VF-1ms column (15 m length, 0.25 mm inner diameter, 0.25 mm d_f) from Varian Instrument group and detected with a flame ionization detector. The column temperature was increased from 90 to 250 °C over 8.5 min, and the temperatures of the injector and detector were held at 250 and 300 °C, respectively. The retention times were 3.1 and 6.3 min for dodecanol and dodecyl decanoate, respectively.

Immobilization and Chemoenzymatic Epoxidation. Native CalB and the M83I and M129L mutants were immobilized on sieved Accurel MP 1000 (250−500 μm). The support was wetted with ethanol (3 mL/g) and thereafter loaded with approximately 20 mg of enzyme/g of support. The support/enzyme mixtures were incubated overnight while being shaken. The supernatant was collected and the enzyme preparation

dried in a vacuum desiccator. The lipases were adsorbed completely, as determined by measuring the residual activity in the supernatant with the esterification assay described above.

The chemoenzymatic epoxidation was performed using 5 mg of immobilized enzyme added to 1 g of rapeseed methyl ester and 320 μL of H_2O_2 (30%, w/w) in a 4 mL vial. Incubation was performed in a thermomixer at 40 °C and 700 rpm, and samples were withdrawn at appropriate intervals (1−24 h). Samples were centrifuged to remove water and weighed, and the oxirane numbers were measured as described previously.[15] After 24 h, the substrate/product mixtures were removed from the enzyme beads by pipetting, and substrates were added for a second batch of chemoenzymatic epoxidation.

RESULTS AND DISCUSSION

To gain some understanding of the effect of oxidation, we have performed MD simulations of wild-type CalB, the enzyme with one or two oxidized amino acid residues, and four mutants (16 simulations in total). The enzyme was equilibrated for 0.5 ns and then simulated for 18 ns, during which time we studied six different properties, viz., the radius of gyration, the rmsd from the starting crystal structure, the average *B* factors of the various residues, the S−S distances of the cystine disulfide pairs, and the hydrogen bond structure of the active site and around the oxidized amino acid. The results of this analysis are described in separate sections below. We also constructed four mutants by site-directed mutagenesis and studied their activity and stability.

Radius of Gyration. The radius of gyration describes the general size of the protein. It indicates global changes in the shape of the protein. The radii of gyration during the simulations are shown in Figure 3, and the average values over the 18 ns

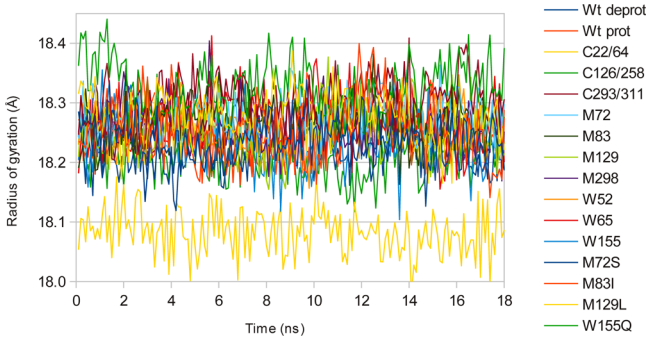

Figure 3. Radii of gyration as a function of time for the various simulations.

production simulations are listed in Table 1. It can be seen that most of the simulations give average radii of gyration of 18.24−18.27 Å. However, the C216/258 and C293/311 simulations give slightly larger radii of 18.32 and 18.31 Å, respectively. This indicates that the oxidations do not have any major impact on the general shape of the protein, except some rather small changes when the cystine disulfide linkages are broken.

For three of the mutants, the radii of gyration are significantly smaller than for the wild-type enzyme. For the M129L mutant, it is 18.08 Å, whereas for the M72S and W155Q mutants, they are 18.21−18.22 Å. These changes are caused by the mutations, because the radius of gyration depends on the mass of the various atoms (the moments of inertia).

rmsd. The rmsd shows how much the structure differs from the starting (crystal) structure. The rmsd during the simulations

Table 1. Average Radii of Gyration and rmsds from the Crystal Structure for the Various Simulations over the 18 ns Simulations

	radius of gyration (Å)	rmsd (Å)
WtD	18.240 ± 0.001	0.760 ± 0.001
WtP	18.254 ± 0.001	0.770 ± 0.002
C22/64	18.271 ± 0.001	0.883 ± 0.002
C216/258	18.321 ± 0.001	1.530 ± 0.002
C293/311	18.305 ± 0.001	1.122 ± 0.001
M72	18.273 ± 0.001	0.750 ± 0.001
M83	18.266 ± 0.001	0.778 ± 0.001
M129	18.247 ± 0.001	0.732 ± 0.001
M298	18.260 ± 0.001	0.950 ± 0.002
W52	18.261 ± 0.001	0.702 ± 0.001
W65	18.270 ± 0.001	0.770 ± 0.001
W155	18.237 ± 0.001	0.797 ± 0.002
M72S	18.222 ± 0.001	0.745 ± 0.001
M83I	18.260 ± 0.001	0.911 ± 0.002
M129L	18.084 ± 0.001	0.737 ± 0.001
W155Q	18.207 ± 0.001	0.679 ± 0.001

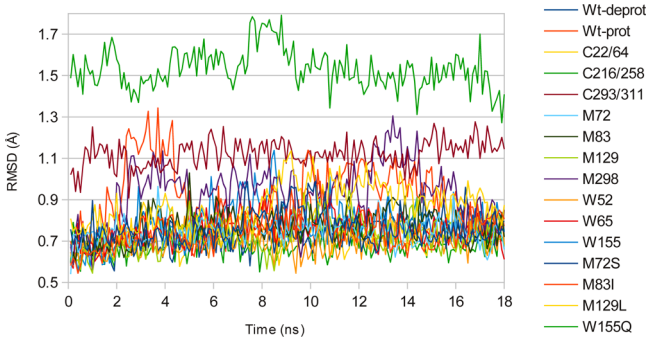

Figure 4. rmsd with respect to the crystal structure as a function of time for the various simulations.

is shown in Figure 4, and Table 1 lists the average over the 18 ns simulations. The flexible loop at the entrance of the active-site cleft, involving residues 140−150, was excluded from the analysis because it showed slow motions even for the wild-type enzyme, which would hide all the other motions of the enzyme. It can be seen that the rmsd shows appreciably larger differences between the various simulations than the radii of gyration. For most of the simulations, including the two wild-type simulations, the rmsd is 0.68−0.80 Å. However, five of the simulations give significantly larger rmsds of 0.88−1.53 Å (note that the standard error is <0.001−0.002 Å). These are the three Cys oxidations, as well as the M298 oxidation and the M83I mutation. These five simulations also show some trends or oscillations in the time course of the rmsd, indicating that the simulations are not fully stable. This clearly shows that the Cys oxidations lead to quite large changes in the structure of CalB.

***B* Factor Analysis.** Next, we studied the average calculated *B* factor of all residues in the protein, to see if there is any increase in the flexibility of certain parts of the structure. The *B* factors are plotted in Figure 5. The plot clearly shows the large flexibility of the solvent-exposed helix formed by residues 140−150 and adjacent residues 282−290. The average *B* factor over the whole protein, except these two sections, is 15−17 Å^2 for all simulations, except the three simulations with Cys oxidations and the M83I mutant, which has slightly higher *B* factors (20−24 Å^2). For the M83I mutant, the differences are essentially

dx.doi.org/10.1021/bi301298m | *Biochemistry* 2013, 52, 1280−1289

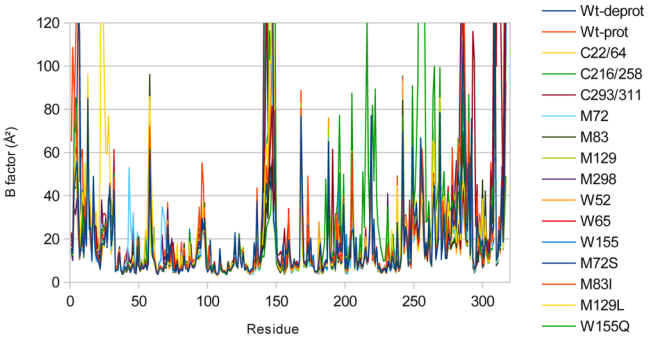

Figure 5. *B* factors for the various residues in CalB calculated over the 18 ns MD simulations. A few large peaks have been truncated to emphasize the typical values.

restricted to a few residues at the start and end of the enzyme (residues 1−10 and 315−317, respectively), probably indicating a variation not induced by the mutation.

On the other hand, the three oxidations of Cys residues give rise to large *B* factors of at least one of the oxidized Cys residues, e.g., by 63 Å^2 for Cys-22 (and 250 Å^2 for Gln-23), 120 Å^2 for both Cys-216 and Cys-258 (and 476 Å^2 for Ile-255), and 116 and 291 Å^2 for Cys-293 and Cys-311. This shows that cleavages of the Cys−Cys links lead to large increases in the flexibility of local environment.

None of the other amino-acid oxidations or mutations lead to any significant increase in the *B* factors of the affected residue (*B* factors of 6−21 Å^2, which are within 8 Å^2 of the results for the wild-type simulation). However, the oxidation of Met-72 leads to an increase in the *B* factor of three neighboring residues (residues 67−69), by up to 29 Å^2. No such effect is seen for the M72S mutant.

S−S Bonds. The distance between the two S atoms in the Cys−Cys links after the oxidation indicates how much the cleavage of the Cys−Cys bridges affects the structure. Our results show that the C22/64 and C293/311 oxidations give rise to rather small changes in the structure: The S−S distances increase from 2.04 ± 0.001 Å to 5.29 ± 0.01 and 5.20 ± 0.01 Å, respectively. However, the C216/258 oxidation leads to a major change in the local structure, with a S−S distance of 12.39 ± 0.03 Å. This shows that the two Cys residues have drifted away after the cleavage of the S−S bond.

Hydrogen Bond Structure of the Active Site. Next, we studied the hydrogen bond structure of the active site in the various simulations. This is probably the most important property, because it shows what effect the oxidations have on the structure of the active site. The results in Table 2 show that there are some differences in the active-site hydrogen bonds. However, the most important interaction, viz., the hydrogen bond between HD1 of His-224 and OD2 of Asp-187 (the atom names follow the convention used in Protein Data Bank crystal structures[34]), shows only small changes between the various simulations. It is present in ∼90% of the structures in all simulations and is complemented in ∼20% of the structures by a hydrogen bond to the other OD1 atom of Asp-187. On the other hand, there is no hydrogen bond between HG of Ser-105 and NE2 of His-224 in any of the simulations. Instead, HG of Ser-105 forms hydrogen bonds with water (68−86% occupancy).

Table 2. Hydrogen Bonds in the Active Site for the Various Simulations[a]

donor	acceptor	WtP	WtD	C22	C216	C293	M72	M83	M129	M283	W52	W65	W155	M72S	M83I	M129L	W155Q
H Ser-105	O Phe-131	31	35	37	40	40	32	29	35	29	32	33	32	40	24	26	36
H Gln-106	OG Ser-105	87	75	84	74	81	88	85	88	74	88	85	83	84	**61**	86	82
HE21 Thr-57	OG Ser-105		2	**27**													
Wat	OG Ser-105	3	**36**		15	8	4	8	3	15	5	7	6	9	13	4	8
HG Ser-105	OD1 Asp-134		24														
HG Ser-105	Wat	84	68	80	85	74	85	81	87	76	81	83	85	76	76	85	76
H Gly-108	O Ser-105	22	22	22	29	23	20	20	21	24	18	23	12	24	24	26	22
Wat	O Ser-105	29	**109**	5	24	**58**	30	32	37	23	28	25	14	21	23	24	33
H Asp-187	O Ala-185		1		8	4	5	3	4	0	8	7	2	5	3	2	4
H Glu-188	OD1 Asp-187	22	16	**59**	41	21	21	17	17	26	17	26	17	40	27	33	23
H Ile-189	OD1 Asp-187	89	91	83	83	85	86	90	87	90	91	87	82	77	76	74	89
H Val-190	OD1 Asp-187	80	76	87	79	86	80	86	80	80	81	86	90	91	90	91	86
HD1 His-224	OD1 Asp-187	16	14	19	**38**	26	15	25	19	15	14	23	17	18	20	18	21
Wat	OD1 Asp-187	6	7	2			7	1	10	2	5	0		0		0	0
HE22 Gln-193	OD2 Asp-187		0	0	**62**	0		0	0	0	0	0					0
HD1 His-224	OD2 Asp-187	90	86	91	84	85	91	88	91	90	89	89	89	93	88	93	91
Wat	OD2 Asp-187	99	98	100	**129**	97	98	99	98	99	102	98	99	98	98	104	94
HE22 Gln-191	O Asp-187	60	65	**28**	**22**	45	60	62	63	72	**17**	35	70	41	71	56	62
Wat	O Asp-187	97	96	**126**	**143**	111	101	100	96	93	97	82	93	117	92	99	92
H His-224	OE2 Glu-188			1	1	1					0	0	0	2	0	3	7
H His-224	Wat	10	9	8	**40**	8	13	14	10	3	12	7	5		1		
Wat	NE2 His-224	71	66	77	51	68	72	67	71	64	70	68	79	72	68	78	72
HE1 Trp-104	O His-224	47	50	41	**3**	55	50	42	44	45	53	41	39	43	38	44	49
Wat	O His-224				**64**												

[a]Listed are hydrogen bonds involving Ser-105, Asp-187, and His-224 with an occurrence of >10% in at least one of the simulations. A hydrogen bond is judged to be present in a snapshot if the donor−acceptor distance is less than 3.0 Å and the donor−H−acceptor angle is larger than 120°. The hydrogen bonds are described by the involved H donor and acceptor atoms with atom names following Protein Data Bank conventions.[34] The listed occurrences are simply the percentages of the 3600 snapshots in which the hydrogen bond is found. Water molecules can have >100% occurrence because more than one water molecule can form hydrogen bonds to the same atom in a specific snapshot. Differences compared to the WtP simulation of >20% are highlighted in boldface.

dx.doi.org/10.1021/bi301298m | *Biochemistry* 2013, 52, 1280−1289

In the WtD simulation, HG of Ser-105 often forms a hydrogen bond to the OD1 atom of the deprotonated Asp-134 residue (occurrence of 24%). NE2 of His-224 also forms hydrogen bonds with water molecules (occurrence of 51−79%) in all simulations.

There are some additional differences between the various structures, but only for hydrogen bonds with relatively low occurrences. The C216/258 simulation shows the largest deviations with a new hydrogen bond between the OD2 atom of Asp-187 and HE22 of Gln-193 (occurrence of 62%), frequent hydrogen bonds between the backbone H atom of His-224 and water molecules (occurrence of 40%), and changed interactions for the O atom of His-224. This simulation, as well as those of oxidized C22/64 and W52, shows a decreased number of interactions between the HE22 atom of Gln-191 and the backbone O atom of Asp-187 (occupancy of 17−28%, compared to 60% in the WtP simulation). C22/59 also shows an increased occurrence of the hydrogen bond between the backbone H atom of Glu-188 and the OD1 atom of Asp-187 (59% compared to 22% for WtP). Both WtD and the C293/311 simulations show an increased occurrence of hydrogen bonds between the backbone O atom of Ser-105 and water molecules (109 and 58%). The four mutants do not show any extensive changes in the active-site hydrogen bond pattern.

Hydrogen Bonds around the Oxidized Residues. Finally, we have compared the hydrogen bond structure around the affected residues of the native protein (WtP) and the simulation of the oxidized or mutated amino acids. The results are listed in Table 3 with separate sections for each oxidized amino acid or mutation.

For the C22/64 simulation, the oxidation introduces new hydrogen bond partners (O1, O2, O3, and HO3 atoms in the oxidized Cys residues) that can form hydrogen bonds that of course are not possible in the wild-type enzyme (these atoms are marked in bold face in Table 3). For the atoms that are present in both simulations, there are some differences in the occurrence of the hydrogen bonds (up to 42% units), but no qualitative differences.

However, for the C216/258 simulation, more extensive changes are observed. In particular, hydrogen bonds involving H of Cys-258 disappear and are replaced by new hydrogen bonds involving the oxidized atoms, as well as a hydrogen bond between O of Cys-258 and Gln-231 or water.

Likewise, the C293/311 simulation shows major changes in the hydrogen bond pattern. First, a new hydrogen bond involving H of Cys-293 and OD1 of Asn-292 appears. Second, a strong hydrogen bond between O of Cys-293 and HE22 of Gln-291 is replaced by hydrogen bonds to water molecules. Third, a strong hydrogen bond between H of Cys-311 and O of Glu-294 is replaced by weaker and more infrequent hydrogen bonds with water. This shows that the oxidized Cys residues become more water-exposed. In addition, several new hydrogen bonds are formed with the oxidized atoms of the two Cys residues.

Among the four Met oxidations, the sulfoxide oxygen atoms (OS in Table 3) of Met-72 and Met-298 form one to three hydrogen bonds with water molecules. The Met-72 simulation also shows other changes in the hydrogen bond structure, involving the H and O atoms. On the other hand, the oxidations of Met-83 and -129 do not lead to any significant changes in the hydrogen bond pattern, and no interactions with the new OS atoms are observed. The reason for this is that these two residues are deeply buried in the protein (cf. Figure 2).

The oxidation of the Trp residues gives rise to a new OH group (HOZ3), which forms hydrogen bonds in all three simulations. However, the occurrence of the hydrogen bonds varies, reflecting the solvent accessibility of the group (Trp-52 buried in the protein, Trp-65 more solvent exposed, and the CZ3 atom directed into the protein, but Trp-155 on the surface of the protein with CZ3 directed into the solvent, cf. Figure 2). For the other atoms in the oxidized Trp residues, there are only rather small differences, the largest being the hydrogen bond between HE1 of Trp-155 and O of Leu-228 (the occurrence decreases from 47 to 13%).

The M72S mutant gives rise to two new hydrogen bonds involving the OH group of the Ser residue and water molecules. In addition, the occurrence of the hydrogen bond between H and O of Pro-68 increases from 19 to 50%. The M83I mutant shows only a fairly small decrease in the occurrence of the hydrogen bond between the H atom and O of Thr-83 (from 49 to 28%), whereas the M129L mutant does not show any significant changes in the hydrogen bond pattern. On the other hand, the W155Q mutation leads to quite extensive changes in the hydrogen bond structure. The hydrogen bond between the HE1 atom of Trp and the O of Gln-291 is replaced by four hydrogen bonds between OE1 of Gln and HE2 atoms and water, OD of Asp-145, and O of Gln-291.

Altogether, the results of the MD simulations indicate that the oxidations of Met and Trp residues have a quite restricted influence on the structure and activity of CalB. On the other hand, oxidations of the Cys residues, implying cleavage of the Cys−Cys linkages, have much larger effects on the enzyme structure and dynamics. In particular, oxidation of the Cys-216/258 pair, and to a smaller extent also the Cys-22/64 pair, is predicted to severely perturb the structure of the active site and therefore probably decrease the activity.

Activity and Stability of CalB Mutants. To further improve our understanding of the influence of oxidized amino acid residues on enzyme activity and stability, some point-mutated variants of CalB were produced on the basis of the MD simulations and our previous studies.[16,17] Because the Cys−Cys linkages are important for the stability of the protein, we concentrated on the Met and Trp residues. The single-point mutation of CalB residue Met-72 has been constructed previously by Patkar et al.[35] using leucine as a substituent. They reported that this mutant displayed a slightly higher oxidative stability, but at the expense of its thermostability. Estell et al.[36] have suggested that replacing Met with Ala or Ser instead of Leu might generate a more active enzyme. As computer modeling indicates that Ser fits better than Ala at this position in CalB (data not shown), we decided to produce the CalB M72S variant. Three additional CalB mutants, M83I, M129L, and W155Q, were provided in purified form by Novozymes A/S.

All enzyme variants showed a lower specific activity than native CalB when assayed for the esterification of decanoic acid with dodecanol, the W155Q mutant having the lowest (5% of native) and M83I the highest (58%) activity (see Table 4). On the basis of residual activities for the enzymes after incubation with H_2O_2 at room temperature and 40 °C, M83I seems to have a somewhat higher thermostability but a slightly lower oxidative stability than the native enzyme (Table 4). On the other hand, M72S showed no activity after being treated with 0.2 M H_2O_2 at 40 °C for 24 h, but it still had 51% activity after incubation for 24 h in 2 M H_2O_2 at room temperature. This decrease in thermostability is consistent with the M72L variant investigated by Patkar et al.[35] The M129L and W155Q mutants

Table 3. Hydrogen Bond Structure Involving the Oxidized Residues in the Simulations of the WtP Protein and the Various Oxidized Residues (Ox)[a]

			occurrence		distance (Å)	
simulation	donor	acceptor	Ox	WtP	Ox	WtP
C22/64	H Cys-22	Wat	**42**	**18**	2.89	2.89
	H Ala-25	**O2 Cys-22**	13		2.87	
	Wat	**O2 Cys-22**	11		2.79	
	HO3 Cys-22	O Ala-25	72		2.63	
	HO3 Cys-22	Wat	18		2.68	
	Wat	O Cys-22	**65**	**42**	2.78	2.76
	H Cys-64	O Ile-34	**21**	**63**	2.92	2.89
	HO3 Cys-64	O Ile-34	96		2.67	
	H Leu-36	O Cys-64	80	91	2.86	2.83
C216/258	H Cys-216	O Ala-212		81		2.85
	H Gly-254	**O1 Cys-216**	6		2.89	
	Wat	O Cys-216	44		2.78	
	H Cys-258	OD1 Asp-257	17		2.86	
	Wat	**O1 Cys-258**	53		2.79	
	Wat	**O2 Cys-258**	53		2.79	
	HO3 Cys-258	Wat	36		2.68	
	HE21 Gln-231	O Cys-258	5		2.85	
	HE22 Gln-231	O Cys-258	28		2.84	
	Wat	O Cys-258	50		2.78	
C293/311	H Cys-293	OD1 Asn-292	43		2.83	
	Wat	**O1 Cys-293**	99		2.79	
	Wat	**O2 Cys-293**	90		2.79	
	Wat	**O3 Cys-293**	10		2.86	
	HO3 Cys-293	Wat	94		2.68	
	HE22 Gln-291	O Cys-293	**2**	**80**	2.86	2.83
	Wat	O Cys-293	86		2.77	
	H Cys-311	O Glu294		89		2.83
	H Cys-311	Wat	30		2.89	
	Wat	**O1 Cys-311**	47		2.79	
	Wat	**O2 Cys-311**	50		2.79	
	HO3 Cys-311	Wat	95		2.68	
	HH21 Arg-309	O Cys-311	8		2.84	
	Wat	O Cys-311	**53**	**99**	2.77	2.78
M72	H Met-72	O Pro-68	1	19	2.92	2.91
	H Met-72	Wat	**47**		2.89	
	Wat	**OS Met-72**	208		2.69	
	HE21 Gln-106	O Met-72	85	80	2.84	2.85
	HG Ser-153	O Met-72	**83**	**62**	2.79	2.81
M83	H Met-83	O Thr-80	38	49	2.88	2.88
	H Ile-87	O Met-83	74	52	2.87	2.90
M129	H Met-129	O Val-101	65	66	2.89	2.88
	H Thr-103	O Met-129	46	45	2.90	2.90
	HG1 Thr-103	O Met-129	6	13	2.86	2.87
M298	H Met-298	OE1 Gln-77	70	85	2.86	2.84
	Wat	**OS Met-298**	253		2.70	
	H Ala-301	O Met-298	76	79	2.87	2.86
	H Arg-302	O Met-298	26	29	2.89	2.91
W52	H Trp-52	OD1 Asn-51	90	91	2.83	2.83
	HE1 Trp-52	O Leu-228	**13**	**47**	2.90	2.88
	HOZ3 Trp-52	O Leu-55	24		2.77	
	H Ser-56	O Trp-52	29	29	2.90	2.90
	HG Ser-56	O Trp-52	97	95	2.71	2.70
W65	H Trp-65	O Thr-21	84	87	2.86	2.85
	HE1 Trp-65	Wat	36	49	2.90	2.88
	Wat	**OZ3 Trp-65**	51		2.81	
	HOZ3 Trp-65	O Pro-63	64		2.75	
	HOZ3 Trp-65	Wat	20		2.79	
	H Thr-21	O Trp-65	35	37	2.91	2.91
	Wat	O Trp-65	20	28	2.80	2.80
W155	H Trp-155	O Ala-151	44	40	2.89	2.90
	HE1 Trp-155	O Ser-150	14	8	2.90	2.90
	HE1 Trp-155	O Gln-291	69	82	2.85	2.83
	Wat	**OZ3 Trp-155**	73		2.81	
	HOZ3 Trp-155	OD1 Asp-145	97		1.62	
	Wat	O Trp-155	70	85	2.77	2.77
M72S	H Met/Ser-72	O Pro-68	**50**	**19**	2.89	2.91
	Wat	**OG Ser-72**	61		2.82	
	HG Ser-72	Wat	44		2.77	
	HE21 Gln-106	O Met/Ser-72	87	80	2.84	2.85
	HG Ser-153	O Met/Ser-72	69	62	2.82	2.81
M83I	H Met/Ile-83	O Thr-80	**28**	**49**	2.88	2.88
	H Ile-87	O Met/Ile-83	63	52	2.89	2.90
M129L	H Met/Leu-129	O Val-101	76	66	2.87	2.88
	H Thr-103	O Met/Leu-129	59	45	2.89	2.90
	HG1 Thr-103	O Met/Leu-129	19	13	2.86	2.87
W155Q	H Trp/Gln-155	O Ala-151	61	40	2.89	2.90
	HE1 Trp-155	O Gln-291		82		2.83
	Wat	**OE1 Gln-155**	146		2.76	
	HE21 Gln-155	OD1 Asp-145	39		2.84	
	HE21 Gln-155	OD2 Asp-145	26		2.84	
	HE22 Gln-155	O Gln-291	79		2.84	
	Wat	O Trp/Gln-155	83	85	2.77	2.77

[a]Only hydrogen bonds with occurrences of >10% in at least one of the simulations are listed. Distances are average distances over the simulations in which the hydrogen bond is present. Donor and acceptor atoms that are present only in the oxidized residue are marked in boldface. Likewise, differences in occurrence between the WT and oxidized simulations of >20% are also marked in boldface.

Table 4. Specific Activities of Native CalB and Four Mutants and Residual Activities after Incubation for 24 h in the Presence of Hydrogen Peroxide

	specific activity (μmol min^{-1} mg^{-1})	residual activity (%), 0.2 M H_2O_2, 40 °C	residual activity (%), 2 M H_2O_2, room temperature
CalB	190.8	75	56
M72S	25.5	0	51
M83I	111.3	85	47
M129L	100.1	9	18
W155Q	10.1	8	54

had a rather low thermostability (8–9% residual activity) after 24 h at 40 °C, but at room temperature, the W155Q mutant had almost the same stability in 2 M H_2O_2 as the native protein, whereas the M129L mutant showed only 18% residual activity (Table 4). The M83I and M129L mutants had higher residual activity than the native enzyme after incubation at 40 °C with 2 M H_2O_2 (37 and 41%, respectively, vs 24% for native enzyme after 4 h).

Native CalB and the M83I and M129L mutants were immobilized by adsorption on Accurel MP 1000 and tested as catalysts in the chemoenzymatic epoxidation of rapeseed methyl ester. W155Q was not considered to be sufficiently active and the in-house constructed M72S to have an overly low specific activity to justify production of the amount needed for immobilization. For chemoenzymatic epoxidation, the native enzyme was the most active, which can be seen in Table 5.

dx.doi.org/10.1021/bi301298m | *Biochemistry* 2013, 52, 1280–1289

Table 5. Conversion (percentage) of Double Bonds during Chemoenzymatic Epoxidation of Rapeseed Methyl Ester Using Native CalB and the M83I and M12L Mutants Immobilized on Accurel MP 1000

	fresh enzyme, 3 h	fresh enzyme, 24 h	reused enzyme, 24 h
CalB	18.7	52.1	2.8
M83I	13.7	32.8	1.4
M129L	14.7	29.4	1.2

All enzymes showed only minor activity when reused, with native CalB having slightly higher remaining activity than the mutants.

As mentioned above, the same four mutants were also studied by MD simulations. The results in Tables 1−3 and Figures 3−5 show that the MD simulations predict rather small changes in these mutants compared to the native enzyme: The M83I mutant showed an increased rmsd from the crystal structure, but mainly at the two ends of the enzyme, which is not expected to affect the activity of the enzyme significantly. Neither of the mutants showed any large changes in the hydrogen bond structure of the active site, besides a 26% decrease in the occurrence of the hydrogen bond between H of Gln-106 and OG of Ser-105 in the M83I mutant. Likewise, we see only small changes in the hydrogen bond pattern around the mutated residues, besides hydrogen bonds involving atoms directly involved in the mutations and a 21−31% change in the occurrence of a hydrogen bond involving the backbone H atom of the mutated residue for the M72S and M83I mutations.

Comparing these results with those obtained from the experimental studies, we can conclude that both studies agree that the changes are only small and quantitative. The largest observed difference is the low activity of W155Q, which is not reflected by any major changes in the hydrogen bonds in the active site. Apparently, a study of the hydrogen bonds is too simple to catch subtle changes in the activity of the enzyme (a 95% decrease in the activity corresponds to an increase in the activation barrier of only 7 kJ/mol). It is possible that simulations of an enzyme−substrate complex instead would yield more information regarding the activity of the mutants;[37] however, it is likely that much more sophisticated methods involving direct calculations of activation barriers would be needed, and it is still not certain that the accuracy such methods would be sufficient to correctly predict changes in the activation energy of ≤7 kJ/mol. On the other hand, both experiments and simulations indicate that the Met and Trp residues are not the main cause of enzyme inactivation. Instead, oxidation of the Cys residues seems to be the most detrimental to activity.

CONCLUSIONS

On the basis of the earlier reports of oxidative deactivation of CalB in the presence of H_2O_2, we have in this study performed MD simulations of CalB in its native state and with one or two oxidized amino acids. The oxidized amino acids were selected from a mass spectrometry-based investigation, showing which amino acids are most prone to being oxidized.[17] The results show that oxidations and cleavages of all three cystine disulfide bridges gave extensive changes in the local structure of the protein, as indicated by the rmsd from the crystal structure, even if the two residues drifted away only in the case of the C216/258 pair. The latter simulation also gave rise to rather large changes in the hydrogen bond structure of the active site and a significant increase in the radius of gyration of the enzyme. We have also looked at the hydrogen bond structure around the oxidized residues, showing that the new polar atoms that arise through the oxidation often form hydrogen bonds with the surroundings, especially if the residues are solvent-exposed. The latter residues often show changes in the hydrogen bonds for the other atoms in the residue as well, but this mainly reflects the increased flexibility of the residue, rather than any extensive changes in the conformation.

In accordance with the results from the MD simulations, single-point mutations of methionine residues had a modest effect on enzyme activity. One variant, M83I, was more stable than the native enzyme when exposed to H_2O_2 under some conditions. The tryptophan variant (W155Q), on the other hand, showed a severe decrease in activity toward the tested substrates. Unfortunately, the variants had neither significantly increased stability toward H_2O_2 nor improved activity or stability during chemoenzymatic epoxidation. MD simulations of the same mutations indicated small changes in the structure of the protein but were unable to predict the observed subtle changes in enzyme activity.

In conclusion, the MD simulations provide clues about the possibilities of mutating certain oxidation-sensitive residues without having a significant impact on the structure and shape of the protein, but single-point mutations of several of those residues did not notably improve the stability of CalB. Moreover, the specific activity of the enzyme was compromised. As the cleavage of the cystine bonds appears to be the major cause of activity loss, it seems difficult to obtain an active and more stable enzyme simply by site-directed mutagenesis. Nevertheless, some approaches could be attempted. The Cys residues themselves need to be preserved because the linkages are important for the stability, but they could be made less solvent accessible by mutating neighboring residues to bulkier groups. Another mutation strategy could be to protect sensitive areas by incorporation of oxidation-sensitive amino acids (e.g., Met residues) to function as protective residues; Met residues on the surface can often be oxidized without any effect on enzyme activity.[16,38,39]

On the other hand, biocatalyst engineering by immobilization of the enzyme on a suitable support may provide a simpler approach for stabilization. Immobilization of CalB on hydrophobic octadecyl Sepabeads[40] and styrene-divinylbenzene beads[41] has been shown to give increased stability toward oxidation by H_2O_2, which could be attributed to shielding of sensitive residues.[40] However, as H_2O_2 is the substrate for the enzyme in chemoenzymatic epoxidation, it is essential that the active site of the immobilized enzyme is still accessible for H_2O_2. This remains to be tested as well as the economic feasibility of the preparation. In conclusion, the results presented here can lay the basis for further stabilization experiments as well as studies to further elucidate the effect of oxidation on biocatalyst activity and stability.

ASSOCIATED CONTENT

Supporting Information

Amber topology and parameter files for the oxidized methionine sulfoxide, cysteic acid, and 5-hydroxytryptophan residues. This material is available free of charge via the Internet at http://pubs.acs.org.

AUTHOR INFORMATION

Corresponding Author

*E-mail: ulf.ryde@teokem.lu.se.

Present Addresses

[‖]Department of Chemistry, University of Kurdistan, Sanandaj, Iran.

[⊥]Center for Process Engineering and Technology, Department of Chemical and Biochemical Engineering, Technical University of Denmark, 2800 Lyngby, Denmark.

Funding

This investigation has been supported by grants from the Swedish Research Council (Project 2010-5025), the FLÄK research school in pharmaceutical science, and Novozymes A/S and Novo Nordisk A/S (Bagsvaerd, Denmark).

Notes

The authors declare no competing financial interest.

■ ACKNOWLEDGMENTS

This investigation has been supported by computer resources of Lunarc at Lund University, NSC at Linköping University, C3SE at Chalmers University of Technology, and HPC2N at Umeå University. Jesper Brask of Novozymes A/S is acknowledged for providing M83I, M129L, and W155Q. M.Sc. student Camilla Melin Fürst is thanked for performing activity and stability measurements.

■ REFERENCES

(1) Bummer, P. M., and Kuppenol, S. (2000) Chemical and physical considerations in protein and peptide stability. *Drugs Pharm. Sci. 99*, 5−69.

(2) Buisman, G. J. H. (1999) Biodegradable binders and cross-linking agents from renewable resources. *Surf. Coat. Int. 82*, 127−130.

(3) Benaniba, M. T., Belhaneche-Bensemra, N., and Gelbard, G. (2003) Stabilization of PVC by epoxidized sunflower oil in the presence of zinc and calcium stearates. *Polym. Degrad. Stab. 82*, 245−249.

(4) Warwel, S., Bruse, F., Demes, C., Kunz, M., and Klaas, M. R. (2001) Polymers and surfactants on the basis of renewable resources. *Chemosphere 43*, 39−48.

(5) Orellana-Coca, C., Törnvall, U., Adlercreutz, D., Mattiasson, B., and Hatti-Kaul, R. (2005) Chemo-enzymatic epoxidation of oleic acid and methyl oleate in solvent-free medium. *Biocatal. Biotransform. 23*, 431−437.

(6) Orellana-Coca, C., Camocho, S., Adlercreutz, D., Mattiasson, B., and Hatti-Kaul, R. (2005) Chemo-enzymatic epoxidation of linoleic acid: Parameters influencing the reaction. *Eur. J. Lipid Sci. Technol. 107*, 864−870.

(7) Orellana-Coca, C., Billakanti, J., Mattiasson, B., and Hatti-Kaul, R. (2007) Lipase mediated simultaneous esterification and epoxidation of oleic acid for the production of alkylepoxystearates. *J. Mol. Catal. B: Enzym. 44*, 133−137.

(8) Björkling, F., Frykman, H., Godtfredsen, S. E., and Kirk, O. (1992) Lipase catalyzed synthesis of peroxycarboxylic acids and lipase mediated oxidations. *Tetrahedron 48*, 4587−4592.

(9) Patkar, S., Björkling, F., Zundell, M., Schulein, M., Svendsen, A., Hansen, H. H., and Gormsen, E. (1992) Purification of two lipases from *Candida antarctica* and their inhibition by various inhibitors. *Indian J. Chem. 32B*, 76−80.

(10) Andersson, E. M., Larsson, K. M., and Kirk, O. (1998) One biocatalyst—many applications: The use of *Candida antarctica* lipase in organic synthesis. *Biocatal. Biotransform. 16*, 181−204.

(11) Uppenberg, J., Hansen, M. T., Patkar, S., and Jones, T. A. (1994) Sequence, crystal structure determination and refinement of 2 crystal forms of lipase-b from *Candida antarctica*. *Structure 2*, 293−308.

(12) Uppenberg, J., Ohrner, N., Norin, M., Hult, K., Kleywegt, G. J., Patkar, S., Waagen, V., Anthonsen, T., and Jones, T. A. (1995) Crystallographic and molecular-modeling studies of lipase B from *Candida antarctica* reveal a stereospecificity pocket for secondary alcohols. *Biochemistry 34*, 16838−16851.

(13) Martinelle, M., Holmqvist, M., and Hult, K. (1995) On the interfacial activation of *Candida antarctica* lipase-A and lipase-B as compared with *Humicola-lanuginosa* lipase. *Biochim. Biophys. Acta 1258*, 272−276.

(14) Blank, K., Morfill, J., Gumpp, H., and Gaub, H. E. (2006) Functional expression of *Candida antarctica* lipase B in *Escherichia coli*. *J. Biotechnol. 125*, 474−483.

(15) Törnvall, U., Orellana-Coca, C., Hatti-Kaul, R., and Adlercreutz, D. (2007) Stability of immobilized *Candida antarctica* lipase B during chemo-enzymatic epoxidation of fatty acids. *Enzyme Microb. Technol. 40*, 447−451.

(16) Törnvall, U., Hedtröm, M., Schillén, K., and Hatti-Kaul, R. (2010) Structural, functional and chemical changes in *Pseudozyma antarctica* lipase B on exposure to hydrogen peroxide. *Biochemie 92*, 1867−1875.

(17) Törnvall, U., Melin Furst, C., Hatti-Kaul, R., and Hedström, M. (2009) Mass spectrometric analysis of peptides from an immobilized lipase: Focus on oxidative modifications. *Rapid Commun. Mass Spectrom. 23*, 2959−2964.

(18) Bas, D. C., Rogers, D. M., and Jensen, J. H. (2008) Very fast prediction and rationalization of pKa values for protein-ligand complexes. *Proteins 73*, 765−783.

(19) Case, D. A., Cheatham, T. E., III, Darden, T., Gohlke, H., Luo, R., Merz, K. M., Jr., Onufriev, A., Simmerling, C., Wang, B., and Woods, R. (2005) The Amber biomolecular simulation programs. *J. Comput. Chem. 26*, 1668−1688.

(20) Wu, X., and Brooks, B. R. (2003) Self-guided Langevin dynamics simulation method. *Chem. Phys. Lett. 381*, 512−518.

(21) Berendsen, H. J. C., Postma, J. P. M., van Gunsteren, W. F., DiNola, A., and Haak, J. R. (1984) Molecular dynamics with coupling to an external bath. *J. Chem. Phys. 81*, 3684−3690.

(22) Darden, T., York, D., and Pedersen, L. (1993) Particle mesh Ewald: An *N*log(*N*) method for Ewald sums in large systems. *J. Chem. Phys. 98*, 10089−10092.

(23) Ryckaert, J. P., Ciccotti, G., and Berendsen, H. J. C. (1977) Numerical integration of the Cartesian equations of motion of a system with constraints: Molecular dyanmics of *n*-alkanes. *J. Comput. Phys. 23*, 327−341.

(24) Hornak, V., Abel, R., Okur, A., Strockbine, B., Roitberg, A., and Simmerling, C. (2006) Comparison of multiple Amber force fields and development of improved protein backbone parameters. *Proteins 65*, 712−725.

(25) Jorgensen, W. L., Chandrasekhar, J., Madura, J. D., Impey, R. W., and Klein, M. L. (1983) Comparions of simple potential functions for simulating liquid water. *J. Chem. Phys. 79*, 926−935.

(26) Schey, K. L., and Finley, E. L. (2000) Identification of peptide oxidation by tandem mass spectrometry. *Acc. Chem. Res. 33*, 299−306.

(27) Besler, B. H., Merz, K. M., and Kollman, P. A. (1990) Atomic charges derived from semiempirical methods. *J. Comput. Chem. 11*, 431−439.

(28) Frisch, M. J., Trucks, G. W., Schlegel, H. B., Scuseria, G. E., Robb, M. A., Cheeseman, J. R., Montgomery, J. A., Jr., Vreven, T., Kudin, K. N., Burant, J. C., Millam, J. M., Iyengar, S. S., Tomasi, J., Barone, V., Mennucci, B., Cossi, M., Scalmani, G., Rega, N., Petersson, G. A., Nakatsuji, H., Hada, M., Ehara, M., Toyota, K., Fukuda, R., Hasegawa, J., Ishida, M., Nakajima, T., Honda, Y., Kitao, O., Nakai, H., Klene, M., Li, X., Knox, J. E., Hratchian, H. P., Cross, J. B., Bakken, V., Adamo, C., Jaramillo, J., Gomperts, R., Stratmann, R. E., Yazyev, O., Austin, A. J., Cammi, R., Pomelli, C., Ochterski, J. W., Ayala, P. Y., Morokuma, K., Voth, G. A., Salvador, P., Dannenberg, J. J., Zakrzewski, V. G., Dapprich, S., Daniels, A. D., Strain, M. C., Farkas, O., Malick, D. K., Rabuck, A. D., Raghavachari, K., Foresman, J. B., Ortiz, J. V., Cui, Q., Baboul, A. G., Clifford, S., Cioslowski, J., Stefanov, B. B., Liu, G., Liashenko, A., Piskorz, P., Komaromi, I., Martin, R. L., Fox, D. J., Keith, T., Al-Laham, M. A., Peng, C. Y., Nanayakkara, A., Challacombe, M., Gill, P. M. W., Johnson, B., Chen, W., Wong, M. W., Gonzalez, C., and Pople, J. A. (2004) *Gaussian 03*, Gaussian, Inc., Wallingford, CT.

(29) Bayly, C. I., Cieplak, P., Cornell, W. D., and Kollman, P. A. (1993) A well-behaved electrostatic potential based method using

charge restraints for deriving atomic charges: The RESP model. *J. Phys. Chem. 97*, 10269−10280.
(30) Seminario, J. M. (1996) Calculation of intramolecular force fields from second-derivative tensors. *Int. J. Quantum Chem. 60*, 1271−1277.
(31) Nilsson, K., Lecerof, D., Sigfridsson, E., and Ryde, U. (2003) An automatic method to generate force-field parameters for hetero-compounds. *Acta Crystallogr. D59*, 274−289.
(32) Wittrup Larsen, M., Hult, K., and Bornscheuer, U. (2008) Expression of *Candida antarctica* lipase B in *Pichia pastoris* and various *Escherichia coli* systems. *Protein Expression Purif. 62*, 90−97.
(33) Bradford, M. M. (1976) Rapid and sensitive method for the quantitation of microgram quantities of protein utilizing the principle of protein-dye binding. *Anal. Biochem. 72*, 248−254.
(34) Protein Data Bank Contents Guide: Atomic Coordinate Entry Format Description. http://www.wwpdb.org/documentation/format33/v3.3.html.
(35) Patkar, S., Vind, J., Kelstrup, E., Christensen, M. W., Svendsen, A., Borch, K., and Kirk, O. (1998) Effect of mutations in *Candida antarctica* B lipase. *Chem. Phys. Lipids 93*, 95−101.
(36) Estell, D. A., Graycar, T. P., and Wells, J. A. (1985) Engineerng an enzyme by site-directed mutagenesis to be resistant to chemical oxidation. *J. Biol. Chem. 260*, 6518−6521.
(37) Karmerlin, S. C. L., and Warshel, A. (2011) The empirical valence bond model: Theory and applications. *WIREs: Computational Molecular Science 1*, 30−45.
(38) Levine, R., Berlett, B. S., Moskovitz, J., Mosoni, L., and Stadtman, E. R. (1999) Methionine residues may protect proteins from critical oxidative damage. *Mech. Ageing Dev. 107*, 323−332.
(39) Davies, M. J. (2005) The oxidative environment and protein damage. *Biochim. Biophys. Acta 1703*, 93−109.
(40) Hernandez, K., and Fernandez-Lafuente, R. (2011) Lipase B from *Candida antarctica* immobilized on octadecyl Sepabeads: A very stable biocatalyst in the presence of hydrogen peroxide. *Process Biochem. (Oxford, U.K.) 46*, 873−878.
(41) Hernandez, K., Garcia-Galan, C., and Fernandez-Lafuente, R. (2011) Simple and efficient immobilization of lipase B from *Candida antarctica* on porous styrene-divinylbenzene beads. *Enzyme Microb. Technol. 49*, 72−78.